RESEARCH ARTICLE | DECEMBER 29 2015

Molecular hydrogen solvated in water – A computational study

Maciej Śmiechowski

J. Chem. Phys. 143, 244505 (2015)
https://doi.org/10.1063/1.4938571

Molecular hydrogen solvated in water – A computational study

Maciej Śmiechowski[a)]
Department of Physical Chemistry, Chemical Faculty, Gdańsk University of Technology, Narutowicza 11/12, 80-233 Gdańsk, Poland

(Received 10 November 2015; accepted 13 December 2015; published online 29 December 2015)

The aqueous hydrogen molecule is studied with molecular dynamics simulations at ambient temperature and pressure conditions, using a newly developed flexible and polarizable H_2 molecule model. The design and implementation of this model, compatible with an existing flexible and polarizable force field for water, is presented in detail. The structure of the hydration layer suggests that first-shell water molecules accommodate the H_2 molecule without major structural distortions and two-dimensional, radial-angular distribution functions indicate that as opposed to strictly tangential, the orientation of these water molecules is such that the solute is solvated with one of the free electron pairs of H_2O. The calculated self-diffusion coefficient of H_2(aq) agrees very well with experimental results and the time dependence of mean square displacement suggests the presence of caging on a time scale corresponding to hydrogen bond network vibrations in liquid water. Orientational correlation function of H_2 experiences an extremely short-scale decay, making the H_2–H_2O interaction potential essentially isotropic by virtue of rotational averaging. The inclusion of explicit polarizability in the model allows for the calculation of Raman spectra that agree very well with available experimental data on H_2(aq) under differing pressure conditions, including accurate reproduction of the experimentally noted trends with solute pressure or concentration. © *2015 AIP Publishing LLC.* [http://dx.doi.org/10.1063/1.4938571]

I. INTRODUCTION

An in-depth understanding of the phenomenon of hydrophobic hydration is of prime importance to our comprehension of such diverse problems as biomolecule hydration and self-organization, transport properties in biological systems, aqueous phase catalysis, and gas clathrate formation, to name but a few. The classical history of the physicochemical studies on the subject begins with the seminal paper by Frank and Evans from 1945, where the term "iceberg formation" was first applied to describe the thermodynamic outcome of the hydration of non-polar molecules.[1] The uniformly negative entropy of transfer of such molecules from the gas phase to an aqueous solution led these authors to a conjecture that water around them must form highly structured patches termed "icebergs" (although the original authors warned from the outset that this by no means implies structural similarity to genuine water ice phase). The term—somewhat unfortunate due to its connotations as it turned out—set the tone for discussing the hydrophobic hydration problem for years to come. Simple molecules considered originally were soon superseded by complex biomolecules, particularly proteins, beginning with the important works of Kauzmann[2] and Némethy and Scheraga.[3] The multitude of experimental, theoretical, and computational works that followed is impossible to quote in a short introduction, but the topic of hydrophobic hydration has been thoroughly reviewed in the recent decades.[4–9]

Perhaps the most important of the later models of hydrophobic hydration is the Pratt–Chandler theory that rigorously applied statistical thermodynamics to describe water-solvated alkanes.[10] While successful in describing small hydrated molecules, its performance was not as good for large molecules hydration, i.e., in the biologically important regime. However, as recently reviewed by Chandler,[5] later developments provided a consistent picture of hydrophobic hydration on different length scales.[11] It turns out that while small molecules do not disturb water's inherent tendency to form a full set of four hydrogen bonds (H-bonds) and the water remains "bulk-like" to a large extent, the H-bond network around a large molecule cannot accommodate it without sacrificing some of the H-bonds and the average number of them is typically three and less rather than four per H_2O molecule; the crossover point between the two regimes is found at solute radius equal ca. 8 Å.[5]

Maybe the most striking example of a small hydrophobic solute is the hydrogen molecule, H_2. This diatomic gas presents as the smallest conceivable molecule and fulfills the criteria for a hydrophobic solute: it possesses no permanent dipole moment, it is only sparingly soluble in water at standard conditions,[12] it exhibits negative entropy of transfer from the gas phase to an aqueous solution (-26 cal mol^{-1} K^{-1}, approximately equal to helium),[1] and it forms clathrate hydrates at high pressure, low temperature conditions, just like the most prominent example, methane.[13,14] Its importance as a future solution to energetic and environmental problems troubling the human civilization is hitherto limited though, due to the still unresolved issue of its efficient storage. Consequently, the clathrate

a)Author to whom correspondence should be addressed. Electronic mail: Maciej.Smiechowski@pg.gda.pl

hydrates of hydrogen and mixed hydrogen–cosolute systems have been the subject of numerous experimental[15–19] and computational studies.[20–27] The clathrate phase diagram,[20,21,23] stability conditions and guest diffusion,[24–27] and structure and cage occupancy[22,26,27] have been thoroughly studied computationally. The experimental work, initially devoted to synthesis of stable clathrates,[18,19] was followed by detailed structural studies of clathrate cages at different occupancies[15,17] and by examination of tetrahydrofuran doping on the clathrate properties.[15,16]

At the same time, aqueous hydrogen—though interesting due to being the clathrate dissociation product and constituting an important model hydrophobic system as remarked above—has not received such careful attention. The experimental studies of the H_2(aq) system were limited to Raman spectra measurements in the stretching vibration range (the Q-branch)[28] and in the rotations region.[29] The former is more suited for detailed investigation as the principal peak location (~4140 cm^{-1}) is way above the vibrational bands of liquid water, unlike the H_2 rotational spectrum which coincides with the water librational band. The rotational Raman spectra were also computed from molecular dynamics (MD) simulations[30,31] and the structure, thermodynamics, and dynamical properties of H_2(aq) were likewise investigated,[32–34] also using *ab initio* MD (AIMD) simulations.[35] We note in passing here that the closely related hydrophobic solute (i.e., the hydrogen atom, H(aq)) was also studied using MD simulations.[36,37] However, though characterized with remarkable anomalies (e.g., ultrafast diffusion in water), this open-shell system is a non-standard hydrophobic molecule and less relevant for immediate needs of determining the efficient ways of hydrogen storage in different thermodynamic conditions.

In this work, we focus on the design and implementation of a novel flexible and polarizable H_2 molecule model for the purpose of aqueous solutions simulations. While not the first attempt at model development for H_2(aq),[22,26,31] the proposed parametrization is the first one to explicitly take into account all important intra- and intermolecular interaction parameters. As the underlying water model we decided to choose Amoeba, a flexible and polarizable multi-purpose force field proved to be very successful in diverse areas of solvation studies.[38] The Amoeba water model[39] adequately reproduces liquid water properties in wide pressure and temperature range.[40,41] Furthermore, the force field was already tested on small hydrophobic solutes dissolved in water[36,42–46] and molecular flexibility and polarizability was deemed crucially important in reproducing the known properties of the methane hydrates.[45] It is also noteworthy that H(aq) has been recently parametrized for Amoeba force field and promising results for the hydration shell structure and diffusion of the solute were obtained.[36] Therefore, it is reasonable to suspect that proper fine tuning of the force field parameters may yield a model of molecular hydrogen suitable for aqueous phase simulations and potentially surpassing the simpler approaches while still being computationally inexpensive.

The performance of the developed model at ambient thermodynamic conditions is illustrated in this work, which is organized as follows: in Sec. II, generic computational details are first given, while the results (Sec. III) are further subdivided into model development details in Sec. III A, brief description of benchmark systems in Sec. III B, description of volumetric properties of H_2(aq) in Sec. III C, details of hydration shell structure in Sec. III D, and dynamical characterization of the solute and the solvent in Sec. III E. Finally, conclusions and prospects for future studies using the present model are presented in Sec. IV.

II. COMPUTATIONAL METHODS

Ab initio calculations of the H_2 molecule and the H_2–H_2O complex were performed using the Gaussian 09 suite.[47] Both single point energy calculations and standard geometry optimizations were employed. The exact level of theory and basis set varied depending on the purpose, as specified below (Sec. III A).

All molecular dynamics simulations were performed using the Dynamic utility from Tinker,[48] employing the Amoeba force field definition of the water molecule[49] and the newly developed H_2 model consistent with this force field, see Sec. III A. While the exact simulation setup varied slightly for different systems, as detailed in Sec. III B, the common parameters are outlined below. The equations of motion were integrated with a modified Beeman algorithm.[50,51] The time step was universally set to 0.5 fs and the production trajectories were saved every 2 fs. The constant temperature (at T = 298 K) and pressure (at P = 1 bar) conditions were maintained by weakly coupling to a thermal bath with a time constant of 0.1 ps for thermostat and 1.0 ps for barostat.[51,52] In the limit of weak coupling, this approach was demonstrated to sample a proper canonical ensemble.[53] Classical Ewald summation techniques[54] were used to calculate the electrostatic interactions due to polarizable atomic multipoles, while the smooth particle mesh Ewald formulation[55] was used to calculate charge–charge interactions. The real space cutoff for electrostatics was set to half the box length for condensed systems and 9.0 Å for gas phase simulations. The van der Waals (vdW) interactions were similarly considered up to a cutoff of half the box length and 12.0 Å, respectively. The convergence criterion for the induced dipoles was set to 10^{-4} D.

III. RESULTS AND DISCUSSION

A. Model development

The Amoeba force field contains, as usual, bonded and non-bonded terms. The former comprise (in the case of molecular hydrogen) only the bond stretching term which is a quartic oscillator in Amoeba. The latter include the electrostatic interactions that are modeled with multipole expansion up to a quadrupole order at each atomic site, the isotropic atomic polarizabilities giving rise to induced molecular dipoles, and the dispersion interactions governed by a buffered 14-7 potential, see Refs. 38, 39, 49, and 56 for details. Each of these parameters for an H atom forming an H_2 molecule was developed independently from *ab initio* calculations, as detailed below. To ensure the consistency of

the new H_2 model with the Amoeba force field, the protocol for the development of force field parameters for small molecules, as outlined in Ref. 56, was closely followed.

To parametrize the bond stretching term, we employed the UCCSD(T)/aug-cc-pVTZ energy profile obtained by calculating the electronic energy of H_2 varying the bond length in 0.05 Å steps. The quartic functional form of bond oscillator specific to Amoeba[39,56] was then fitted to the *ab initio* results around the energetic minimum (0.5–1.1 Å). As seen in Table I, this procedure gave the final values of $k_b = 398.1$ kcal mol^{-1} Å^{-2} and $b_0 = 0.7452$ Å, see supplementary material for a respective plot.[57] A satisfactory agreement with experimental data is obtained in this way, taking into account that the exact equilibrium bond length is 0.7414 Å,[58] while the force constant from spectroscopic measurements[59] is 414.5 kcal mol^{-1} Å^{-2} (the experimental value was rescaled to take into account the usual 0.5 factor missing in the Amoeba U_{bond} definition, see supplementary material).[57]

The electrostatic interactions were modeled following the recommended procedure for parametrizing the Amoeba force field.[56] Namely, the H_2 molecule was first optimized at the MP2/6-311G(d,p) level and the resulting MP2 electron density was used as an input to the GDMA code.[60] The obtained generalized multipoles were rotated to the local reference frame using Tinker's Poledit utility. Next, these initial multipole values were refined by a fit to the MP2/aug-cc-pVTZ electrostatic potential with the Potential utility from Tinker, keeping the low-level monopoles fixed at initial values (i.e., zero). The final optimized monopole, dipole, and quadrupole values are summarized in Table I. The atomic polarizability of each H atom in H_2 was set to the Tinker's recommended value of 0.496 Å^3.[56] Perhaps the best way to compare the present model to experimental data is to calculate molecular properties of an isolated H_2 from the atomic properties. The experimental value of the molecular quadrupole,[61] $|\mathbf{Q}| = \left(Q_{xx}^2 + Q_{yy}^2 + Q_{zz}^2\right)^{0.5}$, is 0.1355 e Å^{-2} compared to 0.1617 e Å^{-2} obtained from the molecular quadrupole tensor using the present model. Similarly, the isotropic molecular polarizability, $\bar{\alpha} = 1/3$ Tr $\boldsymbol{\alpha}$, is calculated as 0.776 Å^3 vs the usually given experimental value 0.79 Å^3.[62] Again, pretty good agreement with experimental data is reached for both molecular properties.

TABLE I. Selected parameters of the molecular hydrogen model developed in this work: bond length, b_0, force constant, k_b, atomic charge, q, atomic dipole, μ, atomic quadrupole, Q, atomic polarizability, α, vdW well depth, ε, and vdW atomic radius, R^0.

Parameter	Value
b_0/Å	0.745 2
k_b/kcal mol^{-1} Å^{-2}	398.1
q/e	0.0
$\mu_x, \mu_y, \mu_z/e$ Å	0.0, 0.0, −0.229 44
$Q_{xx}, Q_{yy}, Q_{zz}/e$ Å^2	0.043 75, 0.043 75, −0.0875
α/Å^3	0.496
ε/kcal mol^{-1}	0.015
R^0/Å	3.406

Finally, van der Waals (vdW) parameters were fitted to the *ab initio* energies of the H_2–H_2O complex obtained from the CCSD(T)/aug-cc-pVTZ single point calculations at multiple points on the potential energy surface (PES). Basis set superposition error was estimated using the standard Counterpoise correction scheme.[63] Following the recent study of an H atom solvated in H_2O,[36] we scanned the PES keeping the H_2O molecule in the xy plane and moving and rotating the H_2 molecule with respect to it in a 5-coordinate space $\zeta = (R, \theta, \phi, \psi, \xi)$ (see Fig. 1 for coordinate definition). In general, the angles were altered in 45° steps (excluding disallowed or redundant values) and for each angular configuration $(\theta, \phi, \psi, \xi)$ the intermolecular separation R was varied from 2.0 Å to 5.0 Å in 0.1 Å steps. A more detailed list of ca. 4000 studied configurations is included in the supplementary material.[57] Both molecules were kept rigid in their equilibrium Amoeba geometries in order to avoid intramolecular energy terms in the interaction energy. Calculations of the potential energy for the same configurations of the complex were also performed with the Tinker's Analyze utility, using the multipole and polarizability parameters as defined above (for H_2) or coming from the original Amoeba force field definition (for H_2O),[49] but keeping the vdW parameters ε and R^0 zeroed for H_2. This allowed us to effectively estimate the electrostatic energy terms only. Knowing that the intermolecular potential energy in the Amoeba force field is the sum of electrostatic (multipole and polarization) and dispersion terms, one may write

$$E_{\text{vdW}}(\zeta) = E_{\text{tot}}(\zeta) - E_{\text{ele}}^{\text{FF}}(\zeta), \tag{1}$$

where E_{tot} is the "exact" total interaction energy as obtained from the high-level *ab initio* calculations and $E_{\text{ele}}^{\text{FF}}$ is the electrostatic energy in the Amoeba force field as obtained above. The resulting E_{vdW} values were then fitted to the functional form of the force field (a buffered 14-7 potential),[39,56] minimizing the root-mean-square deviation between the fitted and the target values. Points on the PES that were too energetically unfavorable (either total energy or target vdW energy >2 kcal mol^{-1}) were excluded from the fitting process, see supplementary material for details of the fit and for representative force field potential energy curves compared with the exact *ab initio* values.[57] The final vdW parameters values (in Amoeba notation) were found to amount $\varepsilon = 0.015$ kcal mol^{-1} and $R^0 = 3.406$ Å, see Table I. This could

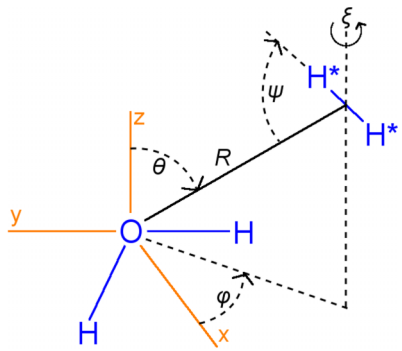

FIG. 1. The internal coordinates, $\zeta = (R, \theta, \phi, \psi, \xi)$, used to define the H_2–H_2O complex geometry for the purpose of potential energy surface scan.

be compared to 0.0206 kcal mol^{-1} and 3.035 Å, respectively, for atomic hydrogen dissolved in water.[36] Interestingly, the converged R^0 value for H in H_2 is very close to the one for water oxygen in the original Amoeba formulation (R^0 = 3.405 Å),[49] while the ε parameter is akin to the one for H_2O hydrogen (ε = 0.0135 kcal mol^{-1}).[49]

The complete molecular hydrogen model developed above for the Amoeba force field is available in the supplementary material in the form of a Tinker key file.[57] We note here that the present effort is by no means the first force field developed for molecular hydrogen for the purpose of studying its solvation in aqueous solutions. Past investigations focused primarily on two models of the H_2 molecule, the simpler one using just a single Lennard-Jones (LJ) interaction site to represent the molecular hydrogen's center of mass. This approach led to parametrization not very different from this work, namely, ε = 0.019 kcal mol^{-1} and R^0 = 3.14 Å.[22] While the latter value seems to differ somewhat from the present one, it is in turn very close to the value for SPC/E water oxygen LJ site, again in accordance with the close similarity to the Amoeba water oxygen case discovered here. Properly capturing the H_2 quadrupole moment in addition to dispersive interactions requires putting point charges in the molecule as well. To ensure the electroneutrality of the entire molecule, this is usually done by placing two equivalent positive charges on the H atoms and a balancing negative charge at the center of mass, together with an LJ interaction site.[26,31] While both approaches have already provided a wealth of data on both aqueous hydrogen and its clathrate hydrates,[21,22,25,26,30–34] the current parametrization is the first one to explicitly take into account all important intra- and intermolecular interaction parameters, at the same time being fully compatible with a well-known force field proved to be very successful in solvation studies.[38] Of course it is entirely possible to achieve parameter-free description of the studied systems by going to the electronic structure theory description and performing fully *ab initio* simulations.[20,23,35] However, even though the increasing computational power available pushes the limits of systems tractable with electronic structure methods, the simulation length and system size as studied here is still not within reach of current resources. Therefore, the developed model can be very useful in predicting the solvation phenomena in aqueous H_2 solutions, as demonstrated below.

B. Benchmark systems

In order to test the newly developed potential, we considered two model systems of relevance to studying molecular hydrogen in its clathrates.

1. Gas phase hydrogen

Gaseous molecular hydrogen at ambient conditions was studied first, mainly in order to deliver reference data for comparison with solvated systems, particularly Raman spectrum. To this end, eight H_2 molecules were placed in a cubic supercell of volume $V \approx 69.06^3$ Å^3, assuming ideal gas conditions at T = 298 K. The system was initially equilibrated for 1 ns in a canonical (*NVT*) ensemble and four independent starting configurations were sampled from this trajectory to initiate 0.5 ns production runs in a microcanonical (*NVE*) ensemble.

2. Aqueous solutions of H_2 at ambient conditions

A starting configuration for aqueous solutions of H_2 was prepared by equilibrating a cubic cell of 444 H_2O molecules for 2 ns in an *NPT* ensemble (at P = 1 bar and T = 298 K). Thereafter, the volume of the box was set to the average of the *NPT* run (discarding initial 1 ns of the trajectory for equilibration) and the system was further simulated in an *NVT* ensemble for 1 ns. The converged box length was $L_0 = 23.702 \pm 0.0092$ Å, corresponding to the liquid density $\rho_0 = 0.998 \pm 0.0012$ g cm^{-3}.

Then, 1, 2, 4, or 8 H_2O molecules with the highest intermolecular separation from immediate neighbors were substituted by H_2 molecules, keeping the initial cell volume intact with respect to the bulk water. Each of the H_2(aq) systems was first equilibrated for at least 2 ns in an *NPT* ensemble simulation in order to relax the box volume (at P = 1 bar and T = 298 K). Next, the volume of the box was set to the average value from the *NPT* run (discarding initial 0.5 ns of the trajectory) and a further 1 ns of equilibration in an *NVT* ensemble was performed. Finally, for the production run, the last *NVT* trajectory was continued and 16 initial conditions were sampled from it every 10 ps in order to initiate *NVE* trajectories of 100 ps length each. All the reported observables (apart from the properties derived directly from the box size) were averaged over the 16 *NVE* runs thus obtaining proper canonical averages.[64] The temperature during the *NVE* simulations experienced no measurable drift and was on average 297.8 ± 0.8 K for the $H_2(H_2O)_{443}$ system.

C. Volumetric properties of H_2(aq)

We initially look in more detail at the concentration-dependent properties of the studied solutions. Note first that even our most diluted solution is well above the solubility limit of H_2 in water, 0.0014 mol. % at T = 298 K,[12] that is ca. 160× less than in the $H_2(H_2O)_{443}$ system. However, as shown in a moment, extrapolation of our finite concentration data to this almost infinite dilution limit is quite possible. As seen in Fig. 2, density of the solutions depends linearly on their molality ($R^2 > 0.999$) and the intercept is in perfect agreement with the bulk water density given above, namely, $\rho^0 = 0.998 \pm 0.0014$ g cm^{-3}. This linear concentration dependence of density is generally expected for moderately diluted non-electrolyte solutions. Basing on the volumetric data, apparent molar volumes of H_2(aq) were calculated directly from the simulations as

$$\Phi_V(H_2) = \frac{V - (444 - n)V^0_{\mathrm{mol}}(H_2O)}{n}, \qquad (2)$$

where V is the system volume with n H_2 molecules and $V^0_{\mathrm{mol}}(H_2O) = 18.06 \pm 0.02$ cm^3 mol^{-1} is the molar volume of the pure water system. The dependence of this quantity on concentration is shown in Fig. 3. The large error bars in Φ_V are

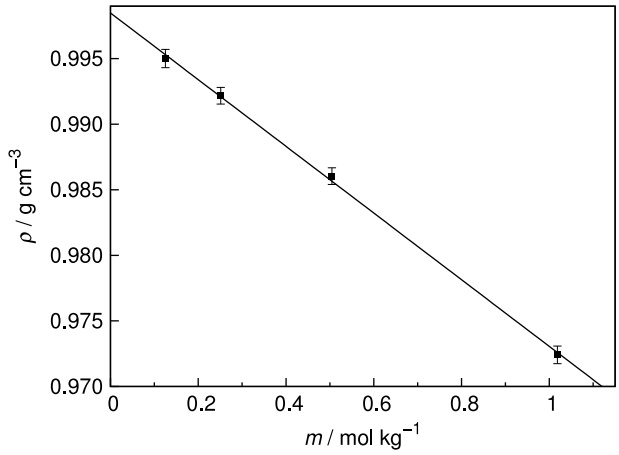

FIG. 2. The dependence of the average density of the studied $(H_2)_n(H_2O)_{444-n}$ systems on the solution molality. Solid line shows the linear least-squares fit, $\rho = -0.025m + 0.998$. Error bars in ρ calculated from the standard error of mean of cell volume.

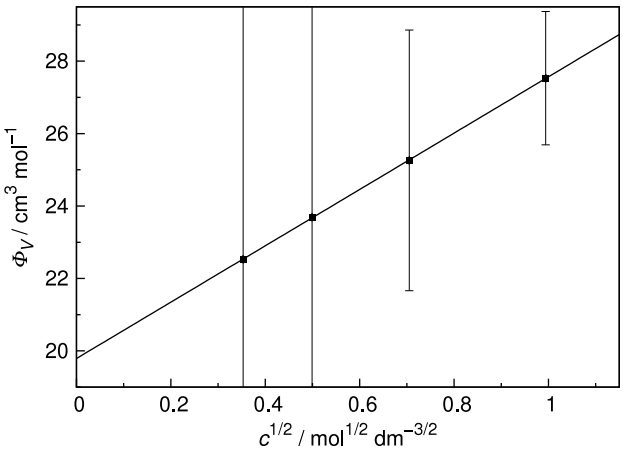

FIG. 3. The dependence of the molar volume of H_2 in the studied $(H_2)_n(H_2O)_{444-n}$ systems on the solution concentration. Solid line shows the linear least-squares fit with Masson equation, Eq. (3). Error bars in Φ_V estimated from Eq. (2). Error bars in $\sqrt{c}$ are smaller than the symbol size.

due to error propagation; this problem is equally well known when working with experimental density data.[65] While there are several known equations for describing the concentration dependence of this quantity, the simplicity of the empirical Masson equation,[66]

$$\Phi_V = V^{\infty}_{\mathrm{mol}} + S_V\sqrt{c}, \tag{3}$$

seems to capture the essential nature of the observed changes, as seen by the excellent quality of the least-squares fit in Fig. 3. Here, S_V is an empirical coefficient and extrapolation to infinite dilution conditions allows for the calculation of the limiting partial molar volume, $V^{\infty}_{\mathrm{mol}}$. The value obtained from the intercept of the line in Fig. 3 is $V^{\infty}_{\mathrm{mol}}(H_2) = 19.8 \pm 0.6$ cm^3 mol^{-1}, very close to the molar volume of pure water. It is also in very good agreement with the most recent estimation based on extrapolating the correlation from Raman spectroscopic data to standard pressure, $V^{\infty}_{\mathrm{mol}}(H_2) = 16.9$ cm^3 mol^{-1}.[28] It is notable that older values available in the literature fall in the range 25–27 cm^3 mol^{-1}.[67,68] However, the present model seems to capture the size effect of the tiny H_2 molecule in accordance with the current experimental data. In contrast to larger model hydrophobic solutes that possess a sizable partial molar volume in water (e.g., $V^{\infty}_{\mathrm{mol}}(CH_4) = 37.3$ cm^3 mol^{-1}),[69] molecular hydrogen readily incorporates into the water network, at least in terms of the occupied volume. This is further illustrated by examining the volume of the Voronoi polyhedron containing the H_2 molecule,[70] which is 31.5 ± 0.4 Å^3 or 21.1 ± 0.3 cm^3 mol^{-1} for the $H_2(H_2O)_{443}$ system, in excellent agreement with the data in Fig. 3.

D. Structure of the H_2 hydration shell in water

1. Radial distribution functions (RDFs)

The average solvation structure is best analyzed in terms of the RDF, $g_{ij}(r)$, which presents spherically averaged density fluctuations of site j with respect to site i. Moreover the running integration of RDF gives the average number of sites j around i and, in particular, yields the coordination number in the first coordination sphere, CN, when integrated up to the first minimum in RDF. The center of mass (CM) of the hydrogen molecule was selected as the reference point to calculate the RDFs for water oxygen and water hydrogen atoms around solvated H_2, $g_{\mathrm{CM-O_w}}(r)$ and $g_{\mathrm{CM-H_w}}(r)$, respectively, as shown in Fig. 4.

The present RDFs are generally in very good agreement with previous MD simulations results,[31,34,35] although the extensive sampling of the configuration space due to the long simulation time applied in this work provides much better statistics and thus smoother curves. The first maximum of the CM–O_w RDF is located at 3.27 Å, while the first minimum at 5.03 Å. The first hydration shell is thus very broad and upon integration one obtains a rather large hydration number, CN = 16.6. Considering the small size of the solute it is apparent that not all of these water molecules interact directly with H_2. Comparison with the CM–H_w RDF reveals very similar values of the first maximum (3.11 Å) and the first minimum (5.35 Å). This is in stark contrast with the electrolyte solutions, where the electrostatic interactions with the ions and

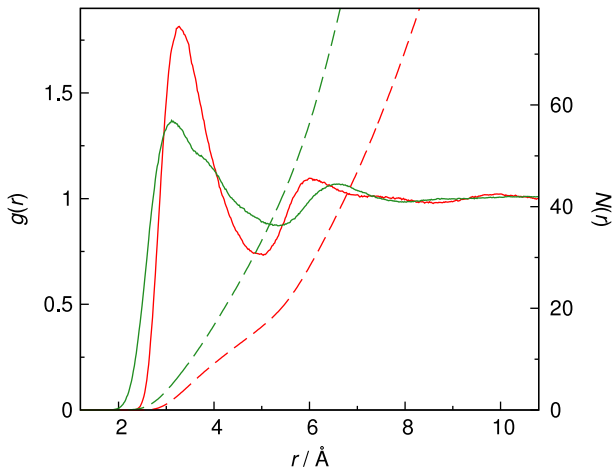

FIG. 4. The radial distribution functions, $g(r)$ (solid lines), and their running integrals, $N(r)$ (dashed lines), for CM–O_w (red) and CM–H_w pairs (green) in the $H_2(H_2O)_{443}$ system.

also H-bonding with the anions cause the water oxygen atoms to be closer to the cations than the hydrogen atoms, while the opposite is true for the anions. The apparent proximity of both maxima observed here strongly suggests that water molecules are positioned in such a way that both hydrogen and oxygen atoms are preferentially located at the same distance from the H_2 CM. This is possible, e.g., with H_2O molecules located tangentially (in terms of their molecular plane) to the intermolecular distance vector as generally postulated for purely hydrophobic solutes.[9] Another interesting feature of $g_{\mathrm{CM-H_w}}(r)$ is the presence of a "kink" in the curve at ca. 3.6 Å. It was previously noted in an AIMD simulation of H_2(aq)[35] and is a consequence of the well-known organization of the hydration sphere of a hydrophobic molecule into two sublayers.[9] This feature is more prominent for the smaller hydrophobic solutes and is usually explained by different orientations of the hydrating water molecules as to best accommodate into the H-bonded network of water, so that the hydrogen atoms of the discussed molecules are tilted either towards the solute or towards the second hydration sphere, resulting in the two observable sub-populations in $g_{\mathrm{CM-H_w}}(r)$.

2. Two-dimensional distribution functions

The above observations about the apparent hydration sphere structuring may be further confirmed by analyzing two-dimensional radial-angular distribution function, $g(r,\beta)$. This approach was already used in the studies of H_2(aq) to show in detail (on the example of water OH bonds orientations) the above-mentioned phenomenon of two sub-populations of H_2O molecules in the first hydration shell.[35] In order to put the stress on the inferred tangential orientation of the nearest water molecules, we selected vector $\boldsymbol{r}$, the intermolecular CM–CM H_2–H_2O distance (with $r = |\boldsymbol{r}|$), and three intramolecular vectors of the water molecule: normal to the H–O–H plane, $\boldsymbol{n}$, the H–H vector, $\boldsymbol{h}$, and the molecular dipole, $\boldsymbol{\mu}$, so that $\beta_1 = \angle(\boldsymbol{r},\boldsymbol{n})$, $\beta_2 = \angle(\boldsymbol{r},\boldsymbol{h})$, and $\beta_3 = \angle(\boldsymbol{r},\boldsymbol{\mu})$, respectively. The probability distributions of all three angles are shown in Fig. 5.

Notably, all the illustrated distributions reveal an intricate structuring of the first hydration shell of H_2 in water. Focusing first on the normal vector $\boldsymbol{n}$, it is obvious that the strictly tangential orientation of water molecules (implying $\angle(\boldsymbol{r},\boldsymbol{n}) = 0°$) is not the most common one. We find the distribution maximum at 3.17 Å and 25°, suggesting that the nearest water molecules are slightly "tilted" with respect to the intermolecular vector. However, the maximum value of $g(r,\beta_1)$ near 0° is only slightly lower and, in general, the β_1 values in the range 0°–45° are preferred than larger ones. Nevertheless, there is a non-negligible population of water molecules located parallel to the intermolecular vector (so that $\beta_1 = 90°$), but more about their detailed orientation (e.g., if the molecular dipole points towards or away from the H_2 molecule) may be inferred from other angular distributions. The surface for $\angle(\boldsymbol{r},\boldsymbol{h})$ shows two maxima within the first hydration shell of approximately equal intensity. They are located at (3.19 Å, 90°) and (3.29 Å, 34°). Interestingly, the former is located more or less at the global maximum of $g(r,\beta_1)$ (regarding r value), suggesting it describes the same subpopulation of the first shell H_2O molecules. Its identity might be further inferred from $g(r,\beta_3)$, which also displays two maxima, this time at (3.21 Å, 66°) and (3.55 Å, 180°). The first one, in combination with the maxima of the two other angles at $r \simeq 3.2$ Å, results in the most probable angular configuration of the water molecules closest to the H_2 molecule. Since in this case $\beta_1 + \beta_3 \simeq 90°$ and furthermore $\beta_2 = 90°$, it immediately follows that the most probable orientation of the immediate water molecules with respect to H_2 is with the H–H intramolecular vector perpendicular to the intermolecular vector and tilted away from the solute by ca. 25°. Note that this makes the H_2 solvated roughly with one of the lone electron pairs on the oxygen atom of H_2O. Perhaps the most surprising is the presence of the other maximum of $g(r,\beta_3)$, namely, at $\beta_3 = 180°$. This corresponds to an anti-parallel orientation of H_2O dipole with respect to the intermolecular vector, i.e., with the molecular dipole pointing directly towards the solute. However, this particular orientation is the least attractive of the possible H_2–H_2O complex arrangements (cf. Fig. S3 in supplementary material).[57] Nevertheless, this has only ~8% smaller intensity than the global maximum at $\beta_3 = 66°$. Additionally, its position is coincident with the observed "kink" in the $g_{\mathrm{CM-H_w}}(r)$ RDF mentioned above and the respective area of higher probability in $g(r,\beta_3)$ extends up

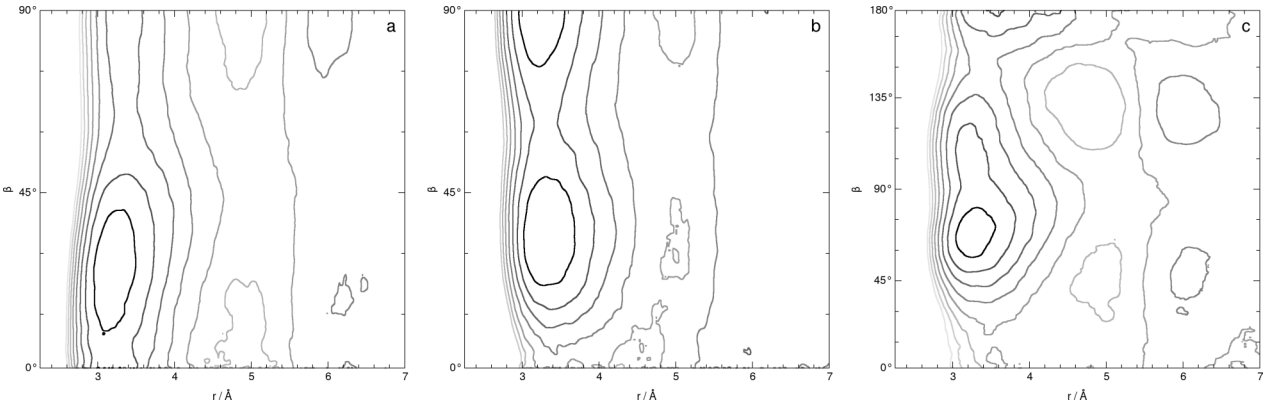

FIG. 5. Two-dimensional probability distribution functions, $g(r,\beta)$, in the $H_2(H_2O)_{443}$ system for: (a) $\beta_1 = \angle(\boldsymbol{r},\boldsymbol{n})$, (b) $\beta_2 = \angle(\boldsymbol{r},\boldsymbol{h})$, and (c) $\beta_3 = \angle(\boldsymbol{r},\boldsymbol{\mu})$, respectively. See text for the definition of vectors. Isolines are drawn on a logarithmic scale for $-\log g(r,\beta) = 1.4$–2.1 in 0.1 log unit steps. Darker contours indicate increasing probability (decreasing $-\log g(r,\beta)$).

to the first minimum of $g_{CM-O_w}(r)$ (cf. Fig. 4). This strongly suggests that the second subshell of the first hydration shell of H_2(aq) is disordered enough to favor even the relatively most repulsive H_2O configurations.

3. Self-association of H_2 in aqueous solution

Finally, we would also like to address the problem of self-association of molecular hydrogen in aqueous solution, as this can potentially alter its hydration shell structure, which is discussed above solely on the example of the $H_2(H_2O)_{443}$ system. As a convenient measure of the degree of this self-association we can again apply the relevant RDF—this time of the CM–CM pairs—and more specifically its running integral, $N(r)$. This is illustrated in a concentration-dependent manner if Fig. 6. It is apparent from this figure, especially for the two larger solute concentrations, that the H_2–H_2 RDFs feature two prominent peaks that may be interpreted as contact associates and solvent-separated associates with increasing r. The first maximum (at 3.11 Å) coincides exactly with the respective maximum in $g_{CM-H_w}(r)$ and suggests rather remote direct contact considering the small size of the solute. The position of the second maximum (at ca. 6.2 Å) is on the other hand roughly equal to twice the CM–O_w distance in the first hydration sphere, as inferred from $g_{CM-O_w}(r)$, confirming single solvent molecule separation in such associates. The degree of association can be measured by integration of $g_{CM-CM}(r)$ up to the first and the second minimum to obtain the average number of contact and (contact + solvent-separated) associates per solute molecule, respectively (N_1 and N_2, see inset in Fig. 6). Both of these numbers depend linearly on molality and the relations have nearly equal zero-crossing, suggesting that below ca. 0.2 mol kg^{-1} solute association is absent in H_2(aq). The linear relationship implies constant degree of association in the studied concentration range. More importantly, low values of N_1 ($\leq$0.2) indicate that solute self-association plays a negligible role at moderate concentrations and should not influence the long-term dynamic and static observables reported here.

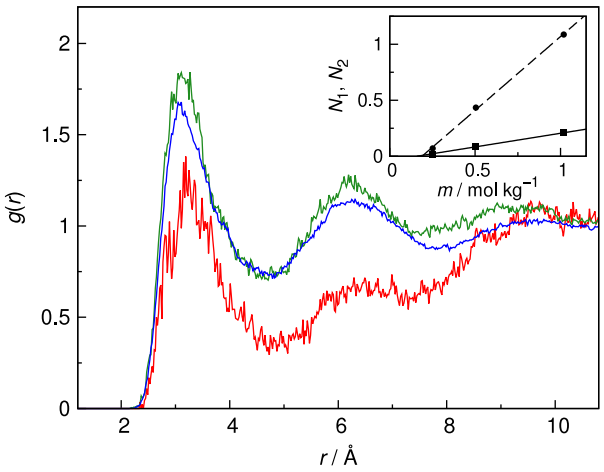

FIG. 6. The CM–CM radial distribution functions, $g(r)$, of the studied $(H_2)_n(H_2O)_{444-n}$ systems for n = 2 (red), n = 4 (green), and n = 8 (blue). (inset) The dependence of the running integrals of $g(r)$ up to the first minimum, N_1 (squares), and the second minimum, N_2 (circles), on the solution molality. Solid and dashed lines show the respective linear least-squares fits.

E. Dynamics of the hydrated H_2

1. Diffusion

It has been known for a long time that small hydrophobic solutes display interesting dynamical properties in an aqueous solution, most notably the "anomalous" fast diffusion, faster than the self-diffusion of H_2O. This is equally true for H_2(aq), however, due to the experimental uncertainties related to its meager solubility in water, the values given for its self-diffusion coefficient at 298 K, D_{H_2}, span a large range from ca. 3 to ca. $7 \cdot 10^{-9}$ m^2 s^{-1}.[71] More recent experiments narrow this range to 3–5 $\cdot 10^{-9}$ m^2 s^{-1},[72,73] i.e., roughly 1.5–2× the self-diffusion coefficient of water ($2.3 \cdot 10^{-9}$ m^2 s^{-1}).[74] The latter qualitative estimate has been often used to gauge the accuracy of MD simulations results.[34,35] Therefore, we first obtain the self-diffusion coefficient of Amoeba water for comparison purposes.

In this work, both mean square displacement (MSD) of the molecular CM and the Green–Kubo approach by integrating the autocorrelation function (ACF) of the CM velocity were used to calculate the self-diffusion coefficients, see Eq. (4),

$$D = \frac{1}{6}\lim_{t\to\infty}\frac{d\left\langle \Delta r^2(t)\right\rangle}{dt} = \frac{1}{3}\int_0^\infty \langle \boldsymbol{v}(t)\boldsymbol{v}(0)\rangle\, dt. \qquad (4)$$

In Table II, the D_{H_2O} values were obtained from the current simulations in order to achieve best consistency with the respective values for H_2. To minimize the solute influence on solvent mobility, only the H_2O molecules outside the first hydration shell of H_2 in the least concentrated system were considered in the ensemble averaging. This exclusion of coordinated water molecules is particularly important, since it is well-known that water molecules in hydrophobic hydration shells diffuse more slowly than in the bulk.[75] Self-diffusion coefficients were calculated by averaging the time derivative of the MSD or the finite integral of the velocity ACF (see Eq. (4)) in the t = 10–60 ps range. The calculated value of D_{H_2O}, ca. $1.7 \cdot 10^{-9}$ m^2 s^{-1}, is approximately 25% lower than the experimental one. More commonly, $D_{H_2O} = 2 \cdot 10^{-9}$ m^2 s^{-1} is given for Amoeba water.[41,49,76] A slightly smaller value ($1.9 \cdot 10^{-9}$ m^2 s^{-1}) was also given in a recent publication.[77] Additionally, a recent determination of this property for a bulk water system of similar size as in this work gave the same value as reported here.[40] Admittedly, the Amoeba

TABLE II. Self-diffusion coefficients obtained from mean square displacement and velocity autocorrelation function, D_{MSD} and D_{ACF} (Eq. (4)) and the respective experimental values, D_{exp}.

Molecule[a]	D_{MSD}	D_{ACF}	$D_{exp}/10^{-9}$ m^2 s^{-1}
H_2	3.10 ± 0.30	3.00 ± 0.10	3.0[b]
H_2O	1.74 ± 0.02	1.71 ± 0.01	2.3[c]

[a]In the $H_2(H_2O)_{443}$ system.
[b]Reference 73.
[c]Reference 74.

water model has an inherent tendency for retarded water mobility, but the deviation from experiment is acceptable and furthermore, the reproduction of trends in experimental self-diffusion coefficients in a wide temperature and pressure range[40] confirms the applicability of the model for predicting mass transport phenomena. The most important potential source of error in our reported D_{H_2O} value is the lack of convergence with respect to system size. This effect is, however, easily taken into account by a size-dependent correction factor $\Delta D = k_B T\xi/(6\pi\eta L)$ for a system with box length L and velocity η, with $\xi \simeq 2.8373$.[78] Substituting the data for the $H_2(H_2O)_{443}$ system (using bulk water viscosity as an approximation, $\eta = 8.9 \cdot 10^{-4}$ Pa s),[79] the correction is found to be $\Delta D = 0.3 \cdot 10^{-9}$ m^2 s^{-1}, making the obtained self-diffusion coefficient exactly equal to the above-cited value $D_{H_2O} = 2 \cdot 10^{-9}$ m^2 s^{-1} that is most commonly given for Amoeba water.

As seen in Table II, the calculated value of D_{H_2} is in excellent agreement with experiment (however, note the rather large range of experimental values as discussed above). Just like D_{H_2O}, it was determined for the $H_2(H_2O)_{443}$ system in order to exclude the possible influence of contact associates present. However, the average self-diffusion coefficients of H_2 determined from the more concentrated systems span the range 2.8–3.2 $\cdot 10^{-9}$ m^2 s^{-1} without any apparent trend with increasing m but rather reflecting the uncertainty of the method. We note here that the Amoeba force field gives also very accurate values of the self-diffusion coefficient of aqueous atomic hydrogen.[36]

At this point, we would like to address the possible impact of nuclear quantum effects (NQEs) inclusion in the present simulations, since H_2 is a molecule for which NQEs are generally suspected to play a non-negligible role. The quantization of the nuclear wavefunction of H_2 as a solute in water was attempted only once via nonadiabatic surface hopping quantum MD to study the influence of NQE on solute transport in a classical solvent bath.[34] While the static solvation structure revealed only slight influence of the NQE inclusion, the self-diffusion coefficient of H_2(aq) was found to increase by ca. 40% upon quantization. Although a substantial increase, this effect is generally comparable to the NQE influence on liquid water itself. While NQE have never been considered explicitly for the Amoeba force field, they well thoroughly studied for another flexible and polarizable water model, TTM2.1-F.[80] It turned out that after NQE inclusion the self-diffusion coefficient of liquid water was found to be ca. 50% greater than its classical counterpart.[81] Although the quantum to classical D_{H_2O} ratio is found to be particularly sensitive to the force field used in the simulations,[82] the TTM2.1-F and Amoeba water models share specific properties (e.g., IR spectrum)[76,81] that strongly suggest the similarity of their dynamic behavior. To conclude, the NQE influence on dynamical properties is suspected to be similar for the solute and for the solvent in the present study. Considering that comparable classical methodologies enjoy a relative success in the elucidation of H_2 clathrate and aqueous solution structure and dynamics,[22,25,26,32,33] the validity of the presented results seems to be well established in spite of neglecting the NQE influence.

Following the analysis from the previous study of H(aq),[36] we also investigate in detail the behavior of the $\Delta r^2(t)$ function in different time regimes in order to characterize the physical mechanism governing the solute MSD over time, see Fig. 7. For the purpose of this figure the $(H_2)_8(H_2O)_{436}$ system was chosen for clarity in order to minimize the noise in $\Delta r^2(t)$ at large t values.

In the short time regime, the motion of H_2 molecules is essentially ballistic, i.e., it is determined by direct collisions with the hydrating water molecules and $\Delta r^2(t) = \langle v_{CM}\rangle^2 t^2$, where $\langle v_{CM}\rangle$ is the average CM velocity of H_2. Accordingly, in this time frame $\Delta r^2(t) \propto t^2$ as seen in Fig. 7. Additionally, we show there the MSD of the H_2 molecules in the studied gas phase system, where the molecular motion is truly ballistic at our conditions close to ideal gas. The perfect correspondence of the aqueous solution and the gas phase MSD time dependence up to ~40 fs confirms the existence of ballistic regime on a time scale characteristic for water librational motion ($\tilde{\nu} \approx 650$ cm^{-1}).

In the long time regime, the steady-state diffusion process governed by Fick laws is dominant and MSD becomes proportional to t. In this regime (at observation time above 10–20 ps), the static self-diffusion coefficient, D_{H_2} as shown in Table II, becomes the relevant property characterizing the diffusion process. Most interesting is, however, the intermediate regime that in the present case of H_2(aq) extends roughly from 0.1–2 ps. In this time period, $\Delta r^2(t) \propto t^\lambda$ with $\lambda < 1$ and this sublinear MSD time dependence is known as dispersive transport and is connected with the emergence of solvent cages trapping the solute before the actual diffusion takes place. In the frequency domain, this time lag corresponds to $\tilde{\nu} \approx$ 10–350 cm^{-1}, i.e., the terahertz (THz) range. It is well known that the vibrational spectrum of liquid water in this range is dominated by the tetrahedral modes of the water H-bond network.[83] This suggests that the cage lifetime is comparable to the lifetime of the local solvation environment of the water molecules. If the fast cavity diffusion were an

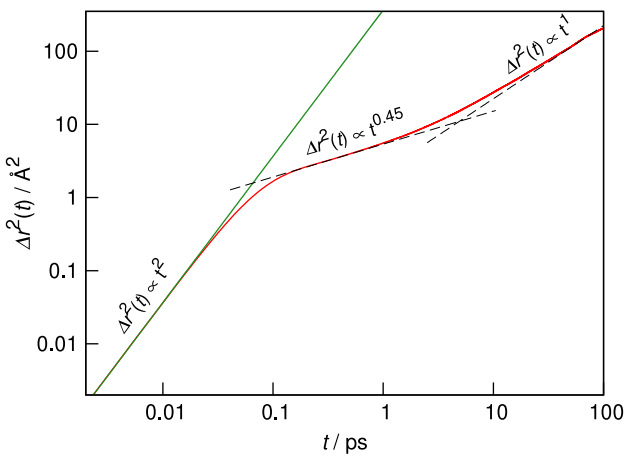

FIG. 7. The dependence of the mean square displacement of CM of H_2 molecules in the $(H_2)_8(H_2O)_{436}$ system (red) and in the gas phase (green) on the correlation time, plotted on a log–log scale. Dashed lines show the approximate behavior in the intermediate time and long time regimes, while labels indicate the t power in the functional dependence of $\Delta r^2(t)$ in each regime.

explanation for increased mobility of H_2 then the intermediate regime would be either very short or non-existent, since cavity would diffuse with the solute and the process would be governed by the long time mechanism.[35] Since $\Delta r^2(t) \propto t^\lambda$ remains true for an extensive part of observation time, a more likely explanation would be some sort of intercage hopping of the solute with the cages being opened by the translational motion of water molecules in the H-bond network or H-bond bending. However, the determination of the activation energy of this process requires additional temperature-dependent simulations.

2. Orientational relaxation

Orientational relaxation in condensed phases is usually described by following the time ACF of the molecular orientation,

$$C_l^\gamma(t) = \langle P_l\left[\boldsymbol{u}^\gamma(t)\boldsymbol{u}^\gamma(0)\right]\rangle, \tag{5}$$

where P_l is the Legendre polynomial of rank l and $\boldsymbol{u}^\gamma$ is the unit vector along the chosen molecular axis γ.[84,85] Of particular importance is the second order $C_2(t)$ function that is experimentally accessible in mid-infrared (IR) pump-probe spectroscopy, while its time integral,

$$\tau_2 = \int_0^\infty C_2(t)\,dt, \tag{6}$$

can be obtained through measurement of the spin-lattice relaxation time in nuclear magnetic resonance (NMR) spectroscopy, although limited time resolution of this technique provides only an average of the molecular reorientation times according to different mechanisms.[86]

For aqueous molecular hydrogen, it was often argued that isotropic intermolecular potential (i.e., single LJ interaction site representing the H_2 molecule CM) is an adequate approximation considering the essentially free rotation of the guest molecule in the solvent cage.[21,22] This isotropic potential was often accompanied by a set of charges reproducing the quadrupole moment of H_2.[26,32] It was found experimentally that in the sII type clathrates the rotational spectrum of H_2 is essentially unchanged with respect to the gas phase spectrum, implying unhindered rotation of the guest molecules.[19] Also first principles calculations support the idea of almost isotropic nature of the H_2–H_2O interactions in this type of clathrates.[25]

For the sake of compatibility with the Amoeba force field our model of the H_2 molecule is fully atomistic (i.e., with atomic quadrupoles and LJ interaction sites) and we would like to check if this changes the conclusions about H_2 rotation in the solvent cages. In Fig. 8, we show the time dependence of the second-rank orientational ACF, $C_2(t)$ (Eq. (5)), again in the $(H_2)_8(H_2O)_{436}$ system in order to minimize the noise in data. The first noteworthy remark is that $C_2(t)$ decays extremely fast in comparison to molecular liquids such as water.[86] However, we also find two regimes in the orientational ACF, as clearly seen by two approximating curves in the figure. At very short times (below 0.04 ps), the orientational ACF shows a clearly Gaussian behavior, $C_2(t) = \exp(-t^2/\tau_G^2)$ with $\tau_G = 0.019 \pm 0.001$ ps. Note that this roughly corresponds to the time regime of ballistic motion of solvated molecules, cf. Fig. 7.

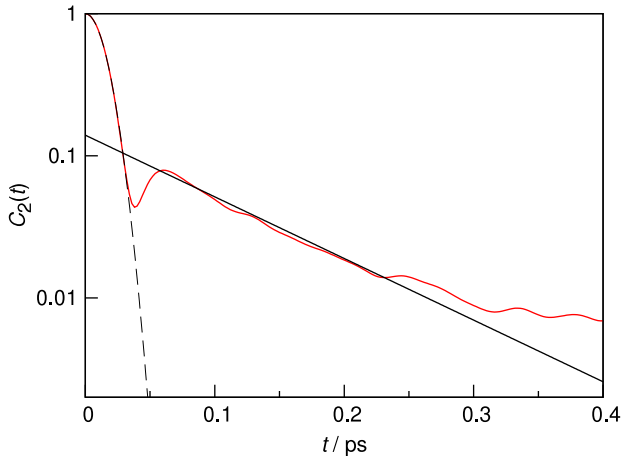

FIG. 8. The time dependence of the second-rank orientational ACF, $C_2(t)$, of the H–H intramolecular vector of H_2 molecules in the $(H_2)_8(H_2O)_{436}$ system (red), plotted on a semi-log scale. Dashed line shows the Gaussian fit at $t < 0.04$ ps, while solid line shows the exponential fit at $0.06 < t\,/\mathrm{ps} < 0.25$.

On a slightly longer time scale, the expected exponential dependence of $C_2(t)$ is evident, although its time constant is much smaller than for typical molecular liquids. Setting $C_2(t) = C_2^\circ \exp(-t/\tau_D)$, we find $\tau_D = 0.10 \pm 0.02$ ps. For comparison, experimental values for bulk liquid water at ambient conditions range from 1.7 to 2.6 ps.[87] For water, $C_2(t)$ reaches its limiting exponential behavior after ca. 1 ps, while for solvated H_2 it is essentially zero (excluding the noise) after the range shown in Fig. 8, i.e., at $t \approx 0.4$ ps the memory of initial orientation is basically forgotten. The average orientational correlation time (irrespective of the mechanism) as defined by Eq. (6) is $\tau_2 = 0.035 \pm 0.005$ ps, again to be compared with ca. 1.5 ps obtained for the rotation of the O–H bond in liquid water.[84] In any case, the obtained values of characteristic rotational correlation times of H_2 in water allow us to conclude that the rotational motion of the solute is essentially decorrelated before reaching the cage boundary in the process of inter-cage transfer, cf. Fig. 7. Therefore, the notion of isotropic nature of the solute–solvent interactions by rotational averaging is highly justified.

3. Isotropic Raman spectra

Raman spectroscopy has been an important tool in studying aqueous solutions of hydrogen gas. The purely rotational Raman spectrum of H_2 in the S-branch (with the selection rule $\Delta J = +2$, where J is the rotational quantum number) coincides with the more intense water librational band, especially the two principal peaks $J = 1 \rightarrow 3$ and $J = 0 \rightarrow 2$ at ~600 and ~350 cm^{-1}, respectively.[29] On the contrary, the H_2 stretching vibration range (i.e., the Q-branch with $\Delta J = 0$) is located above all vibrational transitions of water and recent measurements led to a detailed assignment of the first four rotational levels $Q(J)$ for $J = 0$–3.[28] The location of the principal peak, $Q(1)$, was found to vary linearly with the hydrogen pressure with the limiting value of 4139 cm^{-1} at zero pressure as compared to the gas phase result,

4155 cm^{-1}. Quantitative spectra measurements combined with a simple thermodynamic model gave very accurate results for hydrogen solubility in water and volumetric properties of the solution.[28] The Q-branch Raman spectroscopy was also successfully used in determining the properties of hydrogen clathrate hydrates, with the sII clathrate Q-branch spectrum red-shifted to 4120–4150 cm^{-1} depending on thermodynamic conditions.[19] The H_2 saturated water ice also exhibits a red shift of the Q-branch spectrum by ca. 20 cm^{-1}.[18]

Since the newly developed H_2 model is fully polarizable, we would like to test its applicability to predict Raman spectra of H_2 solutions. The theory behind the computation of Raman spectra from molecular dynamics simulations is well known and routinely applied.[88,89] In the framework of linear response theory, the isotropic Raman spectrum is calculated by Fourier transforming the ACF of the isotropic component of the polarizability tensor ($\bar{\alpha} = 1/3$ Tr $\boldsymbol{\alpha}$), which may be obtained from MD simulations by calculating the electric dipole induced by a static external electric field, see supplementary material for details.[57] Raman spectra calculated for gas phase hydrogen and its aqueous solution are shown in Fig. 9. The spectra were smoothed for presentation by convolution with a Gaussian filter of 5 cm^{-1} width.

Our gas phase spectrum is blue shifted by 180 cm^{-1} with respect to the experiment. In terms of the widely applied scaling concept this corresponds to a scaling factor of 0.9585. The magnitude of this shift is similar to the blue shift of the main ν_{OH} band of H_2O which is found—irrespective of the H_2 concentration—at 3600 cm^{-1} in our calculated solution spectra, while the experimental isotropic spectrum of liquid water has a maximum slightly below 3400 cm^{-1}.[90] The blue shift of the bands with respect to experiment generally reflects too harmonic nature of the underlying fluctuations (here in polarizability), and has been already observed for flexible and polarizable water with a very similar value of the scaling factor.[91] The blue shifts in Raman spectra were then attributed to the absence of the NQE in the simulation. Although the NQE influence on liquid water vibrational spectra is sensitive to the exact treatment of the nuclear motion quantization, in particular, to whether (approximately) fully quantum or mixed quantum-classical approach is used,[92] the quantum IR spectrum of liquid H_2O obtained via centroid MD for the already discussed TTM2.1-F water model clearly exhibits a red shift of the ν_{OH} band by ca. 250 cm^{-1} with respect to the classical spectrum.[81] Therefore, the blue shift of the high-frequency part of the Raman spectrum with respect to experiment as observed in Fig. 9 can be unequivocally attributed to the absence of NQE in our force field, in line with previous statements.[91]

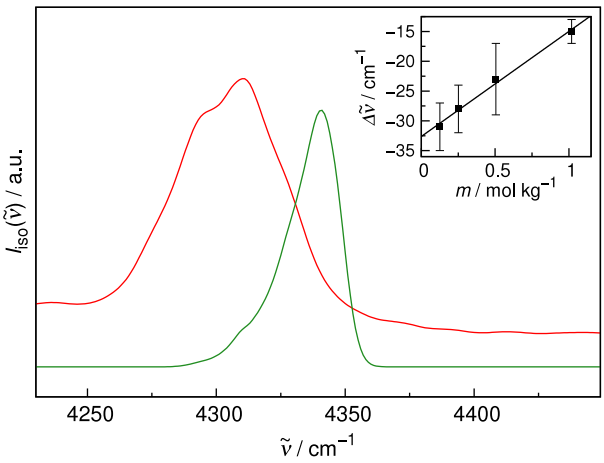

FIG. 9. Isotropic Raman spectra in the H_2 Q-branch range in the $H_2(H_2O)_{443}$ system (red) and in the gas phase (green). (inset) The dependence of the shift of the peak wavenumber at maximum intensity with respect to the gas phase value (4341 ± 1 cm^{-1}), $\Delta\tilde{\nu} = \tilde{\nu}_{aq} - \tilde{\nu}_{gas}$, on the solution molality. Solid line shows the linear least-squares fit.

In any case, observation of the relative trends in the spectra with increasing solute concentration is even more important than absolute quantitative reproduction of experimental results. In the inset of Fig. 9, we show the dependence of the shift of the H_2 Q-branch peak position at maximum intensity with respect to the gas phase value ($\Delta\tilde{\nu} = \tilde{\nu}_{aq} - \tilde{\nu}_{gas}$, with $\tilde{\nu}_{gas}$ = 4341 ± 1 cm^{-1}) on the solution molality. This shift is perfectly linear with molality, in accordance with the experimental data, where a similar relation with respect to the hydrogen pressure was observed.[28] The intercept of this relation, $\Delta\tilde{\nu}^{\infty} = -33 \pm 4$ cm^{-1}, gives the limiting value at infinite dilution. This is ca. 2× larger than the experimental result at zero pressure (−16 cm^{-1}),[28] so that our model exaggerates the relative trends with concentration (or equivalent equilibrium pressure). However, given the errors in the computation of vibrational spectra from MD simulations, such clear reproduction of experimental trends should be considered a success of the present H_2 model.

Since the Q-branch is clearly red-shifted for solvated H_2 with respect to the gas phase, this must imply some change in its polarizability tensor upon solvation, i.e., the existence of intermolecular polarization due to solute–solvent interactions. In search for the origin of this effect, we looked at the induced dipole of molecular hydrogen in aqueous solution. The permanent dipole of H_2 is of course zero, but the polarizability of its atomic sites gives rise to dipoles induced by fluctuating local electric field due to the solvent.[93] We find that the mean value of this induced dipole is μ_{ind} = 0.076 D for aqueous H_2. However, as demonstrated recently for aqueous Na^+, even smaller values of induced dipole can lead to observation of interesting solute–solvent polarization effects in the IR spectra.[94] Here, the seemingly insignificant value of μ_{ind} is found to distinctly alter the isotropic Raman spectrum of H_2(aq) thus revealing the competitive predictive power of polarizable molecular models.

IV. CONCLUSIONS AND OUTLOOK

In the present paper, aqueous hydrogen molecule is studied with molecular dynamics simulations at ambient temperature and pressure conditions. For this purpose, a new flexible and polarizable H_2 molecule model was developed with the aim of maximal compatibility with the Amoeba force field for liquid water. The crucial van der Waals energy component was parametrized by fitting to high level electronic structure calculations of the H_2–H_2O complex, with other components of the model developed according to previous

guidelines. Careful testing of the novel H_2 model proves that it adequately reflects the structural, dynamic, and spectral properties of H_2(aq).

The obtained RDFs are in very good agreement with previous literature reports. Combining them with two-dimensional, radial-angular distribution functions allows us to conclude that the first hydration shell water molecules accommodate the H_2 molecule without major structural distortions and their orientation—as opposed to strictly tangential—is such that the solute is preferentially solvated with one of the free electron pairs of H_2O. The tendency of the solvent to maintain its H-bond network allows the more remote first-shell molecules to adopt even orientations highly unfavorable in the isolated H_2–H_2O complex.

The calculated self-diffusion coefficient of H_2(aq) agrees very well with experimental results. As noted in the previous investigations, it is slightly more than 1.5× larger than for bulk water. Additionally, time dependence of the mean square displacement of H_2 center of mass suggests the presence of caging on a time scale corresponding to hydrogen bond network vibrations in liquid water that is experimentally accessible with THz spectroscopy. Second-rank orientational correlation function of H_2 experiences fast decay on an extremely short time scale, making the H_2–H_2O interaction potential essentially isotropic by virtue of rotational averaging.

The inclusion of explicit polarisability in the model allows for the calculation of Raman spectra that agree very well with available experimental data on H_2(aq) under differing pressure conditions, including accurate reproduction of the experimentally noted trends with the solute pressure. This is made possible by non-negligible dipole induced in H_2 by the solvating water molecules.

The applicability of the present model for calculations of a wide array of structural and dynamic properties of H_2(aq), combined with the already proven ability of the Amoeba force field to reproduce liquid water properties in wide pressure and temperature range, makes it a promising candidate for future studies of the H_2–H_2O system under different thermodynamic conditions, including solid clathrates, hydrothermal solutions, and high hydrostatic pressure conditions.

ACKNOWLEDGMENTS

I want to thank Professor Jan Zielkiewicz for friendly discussions and helpful comments on the first draft of this work. Calculations were performed at ICM Warsaw (Project No. G53-29) and at the Academic Computer Center in Gdańsk (TASK).

[1]H. S. Frank and M. W. Evans, J. Chem. Phys. **13**, 507 (1945).
[2]W. Kauzmann, Adv. Protein Chem. **14**, 1 (1959).
[3]G. Némethy and H. A. Scheraga, J. Chem. Phys. **36**, 3382 (1962).
[4]P. Ball, Chem. Rev. **108**, 74 (2008).
[5]D. Chandler, Nature **437**, 640 (2005).
[6]L. R. Pratt, Annu. Rev. Phys. Chem. **53**, 409 (2002).
[7]V. V. Yaminsky and E. A. Vogler, Curr. Opin. Colloid Interface Sci. **6**, 342 (2001).
[8]P. M. Wiggins, Physica A **238**, 113 (1997).
[9]W. Blokzijl and J. B. F. N. Engberts, Angew. Chem., Int. Ed. Engl. **32**, 1545 (1993).
[10]L. R. Pratt and D. Chandler, J. Chem. Phys. **67**, 3683 (1977).
[11]K. Lum, D. Chandler, and J. D. Weeks, J. Phys. Chem. **103**, 4570 (1999).
[12]E. Wilhelm, R. Battino, and R. J. Wilcock, Chem. Rev. **77**, 219 (1977).
[13]V. V. Struzhkin, B. Militzer, W. L. Mao, H.-K. Mao, and R. J. Hemley, Chem. Rev. **107**, 4133 (2007).
[14]E. D. Sloan, *Clathrate Hydrates of Natural Gases* (Marcel Dekker, New York, 1998).
[15]T. A. Strobel, E. D. Sloan, and C. A. Koh, J. Chem. Phys. **130**, 014506 (2009).
[16]H. Lee, J.-W. Lee, D. Y. Kim, J. Park, Y.-T. Seo, H. Zeng, I. L. Moudrakovski, C. I. Ratcliffe, and J. A. Ripmeester, Nature **434**, 743 (2005).
[17]K. A. Lokshin, Y. Zhao, D. He, W. L. Mao, H.-K. Mao, R. J. Hemley, M. V. Lobanov, and M. Greenblatt, Phys. Rev. Lett. **93**, 125503 (2004).
[18]W. L. Mao and H.-K. Mao, Proc. Natl. Acad. Sci. U. S. A. **101**, 708 (2004).
[19]W. L. Mao, H.-K. Mao, A. F. Goncharov, V. V. Struzhkin, Q. Guo, J. Hu, J. Shu, R. J. Hemley, M. Somayazulu, and Y. Zhao, Science **297**, 2247 (2002).
[20]G.-R. Qian, A. O. Lyakhov, Q. Zhu, A. R. Oganov, and X. Dong, Sci. Rep. **4**, 5606 (2014).
[21]G. S. Smirnov and V. V. Stegailov, J. Phys. Chem. Lett. **4**, 3560 (2013).
[22]S. Mondal, S. Ghosh, and P. K. Chattaraj, J. Mol. Model. **19**, 2785 (2013).
[23]J. Zhang, J.-L. Kuo, and T. Iitaka, J. Chem. Phys. **137**, 084505 (2012).
[24]G. Román-Peréz, M. Moaied, J. M. Soler, and F. Yndurain, Phys. Rev. Lett. **105**, 145901 (2010).
[25]S. Alavi and J. A. Ripmeester, Angew. Chem. **119**, 6214 (2007).
[26]S. Alavi, J. A. Ripmeester, and D. D. Klug, J. Chem. Phys. **123**, 024507 (2005).
[27]S. Patchkovskii and J. S. Tse, Proc. Natl. Acad. Sci. U. S. A. **100**, 14645 (2003).
[28]J. Borysow, L. del Rosso, M. Celli, M. Moraldi, and L. Ulivi, J. Chem. Phys. **140**, 164312 (2014).
[29]D. G. Taylor III and H. L. Strauss, J. Chem. Phys. **90**, 768 (1989).
[30]L. Xiao and D. F. Coker, J. Chem. Phys. **102**, 1107 (1995).
[31]J. E. Hunter III, D. G. Taylor III, and H. L. Strauss, J. Chem. Phys. **97**, 50 (1992).
[32]D. Sabo, S. Varma, M. G. Martin, and S. B. Rempe, J. Phys. Chem. B **112**, 867 (2008).
[33]D. Sabo, S. B. Rempe, J. A. Greathouse, and M. G. Martin, Mol. Simul. **32**, 269 (2006).
[34]H. S. Mei and D. F. Coker, J. Chem. Phys. **104**, 4755 (1996).
[35]B. Kirchner, J. Hutter, I.-F. W. Kuo, and C. J. Mundy, Int. J. Mod. Phys. B **18**, 1951 (2004).
[36]A. Pomogaeva and D. M. Chipman, J. Phys. Chem. B **117**, 16530 (2013).
[37]B. Kirchner, J. Stubbs, and D. Marx, Phys. Rev. Lett. **89**, 215901 (2002).
[38]J. W. Ponder, C. Wu, P. Ren, V. S. Pande, J. D. Chodera, M. J. Schnieders, I. Haque, D. L. Mobley, D. S. Lambrecht, R. A. DiStasio, M. Head-Gordon, G. N. I. Clark, M. E. Johnson, and T. Head-Gordon, J. Phys. Chem. B **114**, 2549 (2010).
[39]P. Ren and J. W. Ponder, J. Comput. Chem. **23**, 1497 (2002).
[40]D. M. Chipman, J. Phys. Chem. B **117**, 5148 (2013).
[41]P. Ren and J. Ponder, J. Phys. Chem. B **108**, 13427 (2004).
[42]N. Galamba, J. Phys. Chem. B **118**, 4169 (2014).
[43]N. Galamba, J. Phys. Chem. B **118**, 2600 (2014).
[44]N. Galamba, J. Phys. Chem. B **117**, 2153 (2013).
[45]F. Castillo-Borja, R. Vázquez-Román, and U. Bravo-Sánchez, Mol. Simul. **34**, 661 (2008).
[46]R. Mahajan, D. Kranzlmüllerr, J. Volkert, U. H. E. Hansmann, and S. Höfinger, Phys. Chem. Chem. Phys. **8**, 5515 (2006).
[47]M. J. Frisch, G. W. Trucks, H. B. Schlegel, G. E. Scuseria, M. A. Robb, J. R. Cheeseman, G. Scalmani, V. Barone, B. Mennucci, G. A. Petersson, H. Nakatsuji, M. Caricato, X. Li, H. P. Hratchian, A. F. Izmaylov, J. Bloino, G. Zheng, J. L. Sonnenberg, M. Hada, M. Ehara, K. Toyota, R. Fukuda, J. Hasegawa, M. Ishida, T. Nakajima, Y. Honda, O. Kitao, H. Nakai, T. Vreven, J. A. Montgomery, Jr., J. E. Peralta, F. Ogliaro, M. Bearpark, J. J. Heyd, E. Brothers, K. N. Kudin, V. N. Staroverov, R. Kobayashi, J. Normand, K. Raghavachari, A. Rendell, J. C. Burant, S. S. Iyengar, J. Tomasi, M. Cossi, N. Rega, J. M. Millam, M. Klene, J. E. Knox, J. B. Cross, V. Bakken, C. Adamo, J. Jaramillo, R. Gomperts, R. E. Stratmann, O. Yazyev, A. J. Austin, R. Cammi, C. Pomelli, J. W. Ochterski, R. L. Martin, K. Morokuma, V. G. Zakrzewski, G. A. Voth, P. Salvador, J. J. Dannenberg, S. Dapprich, A. D. Daniels, Ö. Farkas, J. B. Foresman, J. V. Ortiz, J. Cioslowski, and D. J. Fox, GAUSSIAN 09, Revision D.01, Gaussian, Inc., Wallingford, CT, 2009.
[48]J. W. Ponder, Tinker: Software Tools for Molecular Design, 6.3, Washington University School of Medicine, Saint Louis, MO, 2013.
[49]P. Ren and J. W. Ponder, J. Phys. Chem. B **107**, 5933 (2003).
[50]D. Beeman, J. Comput. Phys. **20**, 130 (1976).
[51]B. R. Brooks, *Algorithms for Molecular Dynamics at Constant Temperature and Pressure* (National Institutes of Health, Bethesda, MD, 1988).

[52]H. J. C. Berendsen, J. P. M. Postma, W. F. van Gunsteren, A. DiNola, and J. R. Haak, J. Chem. Phys. **81**, 3684 (1984).
[53]T. Morishita, J. Chem. Phys. **113**, 2976 (2000).
[54]W. Smith, CCP5 Newsl. **46**, 18 (1998), see http://www.ccp5.ac.uk/infoweb/knowledge_center/smith.pdf.
[55]U. Essmann, L. Perera, M. L. Berkowitz, T. Darden, H. Lee, and L. G. Pedersen, J. Chem. Phys. **103**, 8577 (1995).
[56]P. Ren, C. Wu, and J. W. Ponder, J. Chem. Theory Comput. **7**, 3143 (2011).
[57]See supplementary material at http://dx.doi.org/10.1063/1.4938571 for details of H2 model fitting, TINKER parameter file, and theory of Raman spectra calculations.
[58]*CRC Handbook of Chemistry and Physics*, 88th ed., edited by D. R. Lide (CRC Press, Boca Raton, FL, 2008).
[59]G. Herzberg and L. L. Howe, Can. J. Phys. **37**, 636 (1959).
[60]A. J. Stone, J. Chem. Theory Comput. **1**, 1128 (2005).
[61]A. D. Buckingham, R. L. Disch, and D. A. Dunmur, J. Am. Chem. Soc. **90**, 3104 (1968).
[62]*Landolt–Börnstein Zahlenwerte und Funktionen*, Vol. I, Atom- und Molekülphysik, Teil 3, Molekeln II (Elektronenhülle), edited by A. Eucken, G. Joos, and K.-H. Hellwege (Springer-Verlag, Berlin, 1951), pp. 511–513.
[63]S. F. Boys and F. Bernardi, Mol. Phys. **19**, 553 (1970).
[64]M. Tuckerman, *Statistical Mechanics: Theory and Molecular Simulation* (Oxford University Press, New York, 2010).
[65]Y. Marcus and G. Hefter, Chem. Rev. **104**, 3405 (2004).
[66]D. O. Masson, Philos. Mag. **8**, 218 (1929).
[67]J. C. Moore, R. Battino, T. R. Rettich, Y. P. Handa, and E. Wilhelm, J. Chem. Eng. Data **27**, 22 (1982).
[68]E. W. Tiepel and K. E. Gubbins, J. Phys. Chem. **76**, 3044 (1972).
[69]A. V. Plyasunov and E. L. Shock, Geochim. Cosmochim. Acta **64**, 439 (2000).
[70]C. H. Rycroft, Chaos **19**, 041111 (2009).
[71]D. M. Himmelblau, Chem. Rev. **64**, 527 (1964).
[72]B. Jähne, G. Heinz, and W. Dietrich, J. Geophys. Res.: Oceans **92**, 10767, doi:10.1029/JC092iC10p10767 (1987).
[73]R. N. O'Brien and W. F. Hyslop, Can. J. Chem. **55**, 1415 (1977).
[74]M. Holz, S. R. Heil, and A. Sacco, Phys. Chem. Chem. Phys. **2**, 4740 (2000).
[75]A. Geiger, A. Rahman, and F. H. Stillinger, J. Chem. Phys. **70**, 263 (1979).
[76]L. Wang, T. Head-Gordon, J. W. Ponder, P. Ren, J. D. Chodera, P. K. Eastman, T. J. Martinez, and V. S. Pande, J. Phys. Chem. B **117**, 9956 (2013).
[77]N. Galamba, J. Phys. Chem. B **117**, 589 (2013).
[78]I.-C. Yeh and G. Hummer, J. Phys. Chem. B **108**, 15873 (2004).
[79]Y. Kestin, M. Sokolov, and W. A. Wakeham, J. Phys. Chem. Ref. Data **7**, 941 (1978).
[80]G. S. Fanourgakis and S. S. Xantheas, J. Phys. Chem. A **110**, 4100 (2006).
[81]F. Paesani, S. Iuchi, and G. A. Voth, J. Chem. Phys. **127**, 074506 (2007).
[82]S. Habershon, T. E. Markland, and D. E. Manolopoulos, J. Chem. Phys. **131**, 024501 (2009).
[83]M. Heyden, J. Sun, S. Funkner, G. Mathias, H. Forbert, M. Havenith, and D. Marx, Proc. Natl. Acad. Sci. U. S. A. **107**, 12068 (2010).
[84]S. Chowdhuri and A. Chandra, J. Chem. Phys. **115**, 3732 (2001).
[85]R. W. Impey, P. A. Madden, and I. R. McDonald, Mol. Phys. **46**, 513 (1982).
[86]D. Laage, G. Stirnemann, F. Sterpone, R. Rey, and J. T. Hynes, Annu. Rev. Phys. Chem. **62**, 395 (2011).
[87]D. Laage and J. T. Hynes, Science **311**, 832 (2006).
[88]M. Thomas, M. Brehm, R. Fligg, P. Vöringer, and B. Kirchner, Phys. Chem. Chem. Phys. **15**, 6608 (2013).
[89]Q. Wan, L. Spanu, G. A. Galli, and F. Gygi, J. Chem. Theory Comput. **9**, 4124 (2013).
[90]G. D'Arrigo, G. Maisano, F. Mallamace, P. Migliardo, and F. Wanderlingh, J. Chem. Phys. **75**, 4264 (1981).
[91]T. Hasegawa and Y. Tanimura, J. Phys. Chem. B **115**, 5545 (2011).
[92]M. Rossi, H. Liu, F. Paesani, J. Bowman, and M. Ceriotti, J. Chem. Phys. **141**, 181101 (2014).
[93]S. D. Fried, L. Wang, S. G. Boxer, P. Ren, and V. S. Pande, J. Phys. Chem. B **117**, 16236 (2013).
[94]M. Śmiechowski, J. Sun, H. Forbert, and D. Marx, Phys. Chem. Chem. Phys. **17**, 8323 (2015).